Acta Biochim Biophys Sin 2024, 56(2): 210–222
https://doi.org/10.3724/abbs.2023287
Advance Access Publication Date: 25 January 2024
Original Article

Original Article

lncRNA CYTOR promotes lung adenocarcinoma gemcitabine resistance and epithelial-mesenchymal transition by sponging miR-125a-5p and upregulating ANLN and RRM2

Qijun Cao[1,2,†], Haixia Wang[3,†], Jialong Zhu[1,†], Chen Qi[4,*], Hairong Huang[4,*], and Xiaoyuan Chu[1,*]

[1]Department of Medical Oncology, Jinling Hospital, the First School of Clinical Medicine, Southern Medical University, Nanjing 210016, China, [2]Department of Medical Oncology, Cixi Hospital Affiliated to Wenzhou Medical University, Ningbo 315300, China, [3]Department of Cardiovascular Medicine, Cixi Hospital Affiliated to Wenzhou Medical University, Ningbo 315300, China, and [4]Department of Cardiothoracic Surgery, Jinling Hospital, Medical School of Nanjing University, Nanjing 210093, China

[†]These authors contributed equally to this work.

*Correspondence address. Tel: +86-25-80864770; E-mail: chuxiaoyuan000@163.com (X.C.) / E-mail: huang_hai_rong_01@aliyun.com (H.H.) / E-mail: qichen007@yeah.net (C.Q.)

Received 16 March 2023 Accepted 15 September 2023

Abstract

Lung adenocarcinoma (LUAD) is one of the most aggressive types of lung cancer. The prognosis of LUAD patients remains poor, and the overall efficacy of gemcitabine-based chemotherapy is still unsatisfactory. Long noncoding RNAs (lncRNAs) play important roles in several cancer types by interacting with multiple proteins, RNA, and DNA. However, the relationship between lncRNA dysregulation and gemcitabine resistance in LUAD has not been fully elucidated. In this study, lncRNA CYTOR expression and its association with the prognosis of LUAD patients are assessed by quantitative RT-PCR and Kaplan-Meier survival analysis. *In vitro* and *in vivo* functional studies are conducted to evaluate the biological functions of CYTOR in LUAD. The underlying mechanism regarding the tumor-promoting effects of CYTOR is explored using RNA immunoprecipitation, biotin-labelled RNA pulldown, luciferase reporter assays, and western blot analysis. We identify that CYTOR is an oncogenic lncRNA and is apparently upregulated in LUAD by analysing TCGA-LUAD data. High CYTOR expression is a poor prognostic factor for LUAD. Functional studies reveal that CYTOR confers LUAD cells with stronger resistance to gemcitabine treatment and upregulates the expression levels of epithelial-mesenchymal transition (EMT)-related proteins. Mechanically, CYTOR acts as a competitive endogenous RNA (ceRNA) to absorb miR-125a-5p, weakens the antitumor function of miR-125a-5p, and ultimately upregulates ANLN and RRM2 expressions. Taken together, this study explains the mechanism of lncRNA in the gemcitabine resistance of LUAD and formulates a theoretical framework for the in depth study of LUAD.

Key words CYTOR, lung adenocarcinoma, chemoresistance, miR-125a-5p

Introduction

Lung adenocarcinoma (LUAD) is usually derived from the bronchial epithelium, with some cases originated from the large bronchial mucous glands. LUAD is more likely to occur in women, Asians, and nonsmokers, and the incidence of LUAD has been increasing in recent years [1,2]. Although LUAD typically grows slowly and develops small masses, it easily metastasizes at an early stage and develops resistance to conventional treatment, such as radiotherapy and chemotherapy, which results in poor clinical efficacy and poor prognosis for LUAD patients [3,4]. For LUAD patients with locally advanced or metastatic disease, gemcitabine and gemcitabine-based strategies are the standard chemotherapies [5,6]. Gemcitabine (dFdC) is a pyrimidine antimetabolite that is metabolized into active nucleoside diphosphate (dFdCDP) and nucleoside

triphosphate (dFdCTP) by nucleoside kinase. DFdCDP and dFdCTP inhibit DNA synthesis, thus realizing the cytotoxicity of gemcitabine [7,8]. Despite the clinical efficacy of gemcitabine, it is subject to acquired resistance [9]. Therefore, deeply investigating and understanding the mechanisms underlying gemcitabine resistance in LUAD are crucial to improving its treatment effectiveness.

Long noncoding RNA (lncRNA) is a kind of transcript of more than 200 nucleotides (nt) [10]. LncRNA has limited or no protein-coding capacity but exhibits multifaceted regulatory gene expression in the form of RNA [11]. As research has increased, lncRNA has assumed a greater clinical significance. Aside from controlling embryonic development, lncRNA can also play roles in inflammation, immune cell development, and tumor development [12]. LncRNA has been confirmed as a key biological molecule in tumorigenesis and progression in various human tumors, including liver cancer, breast cancer, head and neck cancer, gastric cancer, and cervical cancer [13–18]. In lung cancer, the prognostic value and crucial effects in cancer development of some lncRNAs have been well verified. For example, a novel risk model containing 12 ferroptosis-related lncRNAs has important prognostic value for LUAD and provides a theoretical basis for the clinical development of ferroptosis-related therapeutic targets [19]. LCAT3 is a recently discovered novel lncRNA that recruits FUBP1 (far upstream element-binding protein 1) proteins to the MYC FUSE (far-upstream element) sequence, activates the transcription of the MYC gene, and ultimately promotes LUAD proliferation, migration, and invasion [20]. The lncRNA CYTOR is highly expressed in various cancers, and CYTOR can partially reverse the suppression of glioma proliferation and migration by UPF1 [21]. CYTOR is also highly expressed in colorectal cancer and predicts poor prognosis [22]. We first found that CYTOR is overexpressed in LUAD by bioinformatics analysis. However, the mechanism of CYTOR in LUAD tumorigenesis and progression needs further exploration.

In the current research, we found that CYTOR is apparently upregulated in LUAD samples compared with adjacent normal tissues by reanalyzing the TCGA-LUAD database. High CYTOR expression indicates a poor clinical outcome in LUAD patients. Gain-of-function and loss-of-function functional experiments verified that CYTOR promotes LUAD cell gemcitabine resistance and epithelial-to-mesenchymal transition (EMT). Mechanically, CYTOR acts as a competing endogenous RNA (ceRNA) to sponge miR-125a-5p, upregulates ANLN and RRM2 expressions, and ultimately plays its pro-oncogenic role in LUAD. Our results shed light on the role of the lncRNA CYTOR in the molecular regulation of LUAD progression and drug resistance.

Materials and Methods

Ethics approval and consent to participate

This study was performed in accordance with the ethical standards of the Declaration of Helsinki and according to national and international guidelines. Our study was approved by the Institutional Ethical Review Board of Jinling Hospital, Nanjing Clinical School of Southern Medical University. Signed consent forms were obtained from all patients.

Cell lines and patient tissues

Human LUAD cell lines (A549, ANIP-973, and NCI-H2122 cells) and a bronchial epithelial cell line (16HBE cells) were obtained from ATCC (Manassas, USA). Cells were routinely cultured at 37°C and 5% CO_2 in RPMI-1640 medium (Gibco, Grand Island, USA) containing 10% fetal bovine serum (FBS; Gibco) and antibiotics (penicillin and streptomycin; Gibco).

This project was granted permission by Jinling Hospital, Nanjing Clinical School of Southern Medical University. LUAD tissues and noncancerous tissues were collected from LUAD patients without any chemo- or radiotherapy before surgical resection. The normal adjacent tissues were paired at a distance of at least 3 cm from the tumor.

Fluorescence *in situ* hybridization

Fluorescence *in situ* hybridization (FISH) was performed as previously described [23]. The FISH signals were detected using the tyramide signal amplification system (PerkinElmer, Waltham, USA) and analyzed with a fluorescence microscope (IX70; Olympus, Tokyo, Japan).

RNA extraction and quantitative RT-PCR

Total RNA was extracted from cells and tissues with an RNA extraction kit (Invitrogen, Carlsbad, USA) according to the manufacturer's instructions. The primers were designed and synthesized by Takara (Dalian, China). The concentration of RNA was measured using a NanoDrop 2000C spectrophotometer (Thermo Fisher Scientific, Waltham, USA). For reverse transcription, 2 μg of total RNA was used to synthesize cDNA using a reverse transcription kit (Qiagen, Hilden, Germany) according to the manufacturer's instructions. The relative expression of miRNAs was measured with *U6* as the internal reference, while other genes (including lncRNAs) were determined with *GAPDH* as the endogenous control. Quantitative RT-PCR experiments were repeated three times in triplicate. Briefly, the reaction was performed according to the following conditions: 95°C for 10 min, followed by 40 cycles of 95°C for 15 s and 58°C for 30 s and 72°C for 30 s. Quantification was performed with the $2^{-\Delta\Delta Cq}$ method. Primers are listed in Supplementary Table S1.

Lentivirus packaging and transduction

293T cells were used to produce lentiviruses. Briefly, 293T cells were seeded in 6-well plates and left to adhere. Purified plasmid DNA with CYTOR overexpression, packaging plasmid psPAX2 and envelope plasmid VSV-G (at a ratio of 1:1:1) were transfected into 293T cells using lipo3000 (Sigma-Aldrich, St Louis, USA). Twelve hours later, the culture medium was refreshed, and the cells were incubated for another 48 h to produce lentivirus. The medium was collected, snap-frozen in liquid nitrogen, and transduced into A549 cells supplemented with polybrene (4 μg/mL; Sigma-Aldrich). Twelve hours later, the culture medium was replaced by RPMI-1640 containing 10% FBS and incubated for another 48 h. Cells were selected with 10 μg/mL puromycin (Thermo Fisher Scientific), and stable clones were saved for subsequent experiments. For shRNA transfections, cells were transfected with sh-CYTOR (Supplementary Table S2) plasmids (4 μg) and their corresponding control vectors with Lipofectamine 3000 Transfection Reagent (Invitrogen) according to the manufacturer's instructions, and harvested for assays 48 h after transfection.

Cell viability assay

Cell viability under gemcitabine treatment was detected using the

cell counting kit 8 (CCK-8) (Dojindo, Kumamoto, Japan). Cells were digested accordingly and diluted to a concentration of 1×10^4 cells/mL. Then, 2000 cells were seeded in each well of 96-well plates and incubated for 24 h. The cells were treated with a concentration gradient of gemcitabine (0, 0.5, 1, 2, 4, 8, and 16 μg/mL) and cultured for 72 h. Then, 20 μL of CCK8 reagent was added to each well and incubated for 4 h. Then the absorbance of each well was detected at 450 nm with an iMark microplate absorbance reader (Bio-Rad, Hercules, USA).

Colony formation assay

A cell colony formation assay was performed to assess the colony formation ability of LUAD cells. In brief, the cell concentration was adjusted to 1×10^4 cells/mL after trypsin digestion, and cells were seeded in triplicate in a 6-well plate (600 cells per well). Then cells were incubated for approximately two weeks at 37°C in a 5% CO_2 incubator to form clones. The colonies were washed with ice-cold PBS, fixed with methanol, and stained with hematoxylin-eosin (H&E). The images of colonies were captured with a Canon camera (Canon, Tokyo, Japan) and the number of colonies in each well was counted.

Western blot analysis

Protein expression in LUAD cells was measured by western blot analysis. Briefly, cells were lysed with radioimmunoprecipitation assay (RIPA) protein lysis buffer containing protease inhibitors (cOmplete™ Protease Inhibitor Cocktail; Sigma-Aldrich) and phosphorylase inhibitor (Sigma-Aldrich). The protein concentration was quantified using the BCA Protein Quantitative kit (Thermo Fisher Scientific) according to the manufacturer's instructions. For western blot analysis, 20 μg of total protein per sample was separated by 4% SDS-PAGE and transferred to nitrocellulose membranes (Millipore, Billerica, USA). The membrane was blocked with 5% nonfat milk buffer for 30 min at room temperature. Then, the primary antibodies, including anti-Vimentin (1:1000, ab8978; Abcam, Cambridge, UK), anti-N-cadherin (1:1000, ab18203; Abcam), anti-E-cadherin (1:1000; Abcam), and anti-GAPDH (1:5000; Abcam), anti-ALNL (1:1000, ab211872; Abcam), anti-RRM2 (1:1000, ab172476; Abcam) were incubated with the membranes at 4°C overnight. After wash with 1× PBST, the membranes were incubated with horseradish peroxidase (HRP)-conjugated secondary antibodies (KS001, KS002; Nanjing Jiancheng Bioengineering Institute, Nanjing, China). Finally, the targeted bands were detected using an enhanced chemiluminescence reagent (Millipore) and photographed and quantified using an imaging system (Thermo Fisher Scientific)

Dual-luciferase reporter assay

The luciferase reporter vector pair-GLO was used to construct luciferase. The miR-125a-5p target sequences of ANLN (ANLN WT), RRM2 (RRM2 WT), or the corresponding mutation sequences (ANLN MUT and RRM2 MUT) were fused downstream from a firefly luciferase expression cassette. Renilla luciferase was used for normalization. Dual-luciferase reporter assays were conducted using a dual-luciferase reporter assay kit (Promega, Madison, USA). LUAD cells in 24-well plates were cotransfected with miR-125a-5p mimic or mimic control and the luciferase reporter vectors. After 48 h of incubation, the cells were lysed with lysis buffer, and the luciferase activity was measured using a luciferase assay system (Promega) according to the manufacturer's instructions.

RNA immunoprecipitation (RIP)

RNA immunoprecipitation was performed using the Magna RIP™ RNA-binding protein immunoprecipitation kit (Millipore). Briefly, cells in 10-cm plates were washed twice with ice-cold PBS and lysed in 1 mL of RIP lysis buffer (0.5% NP-40, 100 mM KCl, 10 mM HEPES, 5 mM $MgCl_2$, 1 mM dithiothreitol, RNA inhibitors, and protease inhibitors, pH 7.0). The protein A/G dynal beads (Thermo Fisher Scientific) were incubated with anti-Ago2 antibodies (5 μg; Abcam) or normal anti-rabbit IgG (5 μg, negative control) for 2 h at room temperature. Then, the cell lysate was centrifuged for 10 min at 4 °C, and the supplement was collected and used for immunoprecipitation to pull down the RNAs in the RISC complex. After overnight incubation, the unbound RNAs were washed off with RIP wash buffer, and the target RNAs were extracted with TRIzol reagent (Thermo Fisher Scientific), followed by quantitative RT-PCR analysis. The input sample (10% from cell lysates) was used to calculate the relative enrichment.

Biotin-labelled miRNA pulldown assay

The biotin-labelled miRNA pulldown assay was performed using a Magnetic RNA-protein pulldown kit (Thermo Fisher Scientific), with some modifications to the manufacturer's instructions. The biotin-labelled miR-125a-5p (5′-UCCCUGAGACCCUUUAACCUGUGA-3′) and the control probes (5′-AACGCTTCACGAATTTGCGT-3′) were purchased from RiboBio Company (Guangzhou, China). Briefly, biotin-labelled miR-125a-5p or the control probes were transfected into LUAD cells at a final concentration of 30 nM. After incubation for 48 h, the cells were lysed using RIPA lysis buffer containing RNase inhibitors and centrifuged at 10,000 *g* for 10 min. To capture the mRNA bound to miR-125a-5p, the supernatant was incubated with streptavidin beads for 30 min with agitation at room temperature. Then, the unbound RNAs were washed off with 100 μL of wash buffer three times. Total RNA was isolated using 50 μL elution buffer, and the RNA eluates were analyzed by quantitative RT-PCR.

Tumor xenograft model

A subcutaneous transplantation tumor model was established to assess the growth and gemcitabine sensitivity of A549 cells *in vivo*. A total of 1×10^6 A549 cells with CYTOR overexpression or control cells were collected and resuspended in RPMI-1640 medium with 10% Matrigel. The cells were subcutaneously injected into the right armpit of nude mice (five mice per group). To assess gemcitabine treatment sensitivity, 10 mg/kg gemcitabine was intraperitoneally injected into the nude mice every 3 days, with PBS as a mock treatment control. The tumor volume was measured every week and calculated according to the formula: length × width^2/2. On day 42, the mice were sacrificed, and the tumors were collected and weighed. All tumors were fixed with 4% paraformaldehyde, paraffin-embedded, and cut into sections (4 μm). The sections were stored at –20°C until analysis.

Immunohistochemical (IHC) and TUNEL staining

Immunohistochemical staining of the xenograft tumor was performed on the paraffin-embedded sections. In brief, the sections were dewaxed and rehydrated. For antigen retrieval, the sections were treated with Tris/EDTA at 98°C for 30 min by microwave

heating and cooled to room temperature naturally. The sections were incubated in 30% hydrogen peroxide buffer for 20 min to inactive endogenous peroxidase. Then, the sections were blocked using PBS supplemented with 5% normal goat serum at room temperature for 30 min. Then, the sections were incubated with anti-Ki67 (ab16667; Abcam) or anti-PCNA (ab29; Abcam) antibodies diluted in blocking solution at 4°C overnight, followed by incubation with biotinylated secondary antibody for 1 h at room temperature. The sections were then treated with streptavidin-conjugated HRP (CSB-PA644737, CSB-PA489724; CUSABIO, Wuhan, China) for 20 min. The staining intensity was detected using diaminobenzidine (DAB; Dako, Glostrup, Denmark). TUNEL staining was conducted with a DeadEnd Fluorometric TUNEL system (Promega) according to the manufacturer's protocol. The results were visualized under an X51 inverted microscope (Olympus, Tokyo, Japan).

Statistical analysis

Data are shown as the mean ± standard deviation (SD) and were analyzed using SPSS software (IBM, Armonk, USA) or GraphPad Prism (GraphPad, La Jolla, USA). All experiments were conducted at least three times. Comparison between two groups were performed using paired or unpaired Student's *t*-test. Multigroup data analysis was performed using one-way ANOVA. Survival curves were generated and analyzed using the Kaplan-Meier method. $P < 0.05$ was considered statistically significant.

Results

lncRNA CYTOR is abnormally upregulated in LUAD and correlated with clinical outcome

In an attempt to explore the lncRNAs that showed strikingly abnormal expressions in LUAD tissues, we reanalyzed the unpaired TCGA-LUAD dataset and found that CYTOR is one of the significantly overexpressed lncRNAs in LUAD tissues compared with adjacent normal tissues (Figure 1A, $P < 0.001$). These results were concordant when we further looked for the paired TCGA-LUAD dataset (Figure 1B, $P < 0.001$). To confirm the results from the TCGA dataset, we collected 8 cases of LUAD cancerous tissues paired with noncancerous counterparts, and the results of quantitative RT-PCR agreed with those from the TCGA dataset (Figure 1C). Furthermore, CYTOR was overexpressed in LUAD tissues compared with normal tissues as revealed by *in situ* hybridization technology in the collected samples (Figure 1D). Kaplan-Meier survival analysis demonstrated that patients with higher CYTOR expression had significantly worse overall survival (Figure 1E, $P < 0.05$), and a higher LHX2 level was significantly associated with T, N and TNM staging (Table 1, $P < 0.05$). Similar results could be found in the LUAD cell lines (A549, ANIP-973, and NCI-H2122) in comparison with the human bronchial epithelial cell line 16HBE (Figure 1F). To evaluate whether a high expression level of CYTOR is clinically important, we analyzed the correlation between CTTOR expression and T stage, N stage, and pathological stage in LUAD patients based on TCGA samples. Not surprisingly, CYTOR expression was positively associated with LUAD T stage (Figure 1G, $P < 0.01$), N stage (Figure 1H, $P < 0.01$) and pathological stage (Figure 1I, $P < 0.01$). Additionally, we performed a Kaplan-Meier survival analysis using the above TCGA dataset, in which LUAD patients were grouped based on CYTOR median expression (high CYTOR and low CYTOR expression). A significant correlation was observed between high CYTOR expression and overall survival (Figure 1J, $P < 0.01$), disease-specific survival (Figure 1K, $P < 0.05$), and progression-free survival (Figure 1L, $P < 0.05$). ROC curves showed that the area under the receiver operating characteristic curve (AUC) value for CYTOR expression was 0.877, with a 95% confidence interval (CI) of 0.831–0.924 (Figure 1M). These results verified that CYTOR expression was significantly increased in LUAD and could serve as a prognostic biomarker for LUAD patients.

CYTOR boosts gemcitabine resistance of LUAD cells and EMT *in vitro*

Since CYTOR is highly expressed in LUAD, we assumed that it has potential tumor-promoting effects. To verify our hypothesis, we initially overexpressed CYTOR in A549 cells and knocked down *CYTOR* in ANIP-973 cells using a short hairpin RNA (shRNA)-mediated gene silencing system (sh-CYTOR#1 and sh-CYTOR#2). Quantitative RT-PCR was used to ensure gene interference efficiency (Figure 2A). To assess the capacity of CYTOR to promote a gemcitabine-resistant phenotype, we exposed A549 and ANIP-973 cells to a gradient of gemcitabine concentrations ranging from 0 to 16 μg/mL for 72 h and measured cell viability by CCK-8 assay. The results showed that CYTOR overexpression confers the capacity for gemcitabine resistance in A549 cells (Figure 2B). Conversely, silencing of *CYTOR* enhanced the response to gemcitabine in ANIP-973 cells (Figure 2C). We then treated LUAD cells with 1 μg/mL gemcitabine and conducted colony formation assay. The results showed that the clone clusters of A549 cells overexpressing CYTOR were larger and more numerous than those of the control cells, indicating gemcitabine resistance in these cells (Figure 2D, upper panel, $P < 0.01$). Meanwhile, *CYTOR* knockdown resulted in a reduction in colony number in ANIP-973 cells (Figure 2D, lower panel, $P < 0.01$).

Available evidence confirms that one of the key hallmarks of EMT is resistance to cell apoptosis, thereby promoting resistance to chemotherapy. Moreover, EMT is a prerequisite for cancer cells to become highly metastatic, and it occurs as a result of dysregulated expressions of EMT-related proteins, such as vimentin, N-cadherin, and E-cadherin. We therefore tested whether CYTOR expression has an influence on the EMT phenotype. We conducted western blot analysis to assess the expression levels of EMT-related proteins in LUAD cells with CYTRO overexpression or knockdown. As expected, the overexpression of CYTOR strongly upregulated N-cadherin and Vimentin expressions, while E-cadherin showed significant downregulation in CYTOR-overexpressing cells (Figure 2E, left panel). In contrast, the knockdown of *CYTOR* produced the opposite result (Figure 2E, right panel). The above results validated that CYTOR promoted LUAD cell progression and chemoresistance *in vitro*.

CYTOR functions as a miRNA sponge to adsorb miR-125a-5p

Mounting studies have demonstrated that lncRNA can act as miRNA sponge molecules (competing endogenous RNA, ceRNA) that adsorb miRNAs to regulate gene expression [24]. Based on this theory, we hypothesized that CYTOR might serve as a miRNA sponge. Thus, we used the DIANA tool (http://diana.imis.athena-innovation.gr/DianaTools/index.php) to search for lncRNA-linked miRNAs to predict CYTOR-targeted downstream miRNAs, where 51

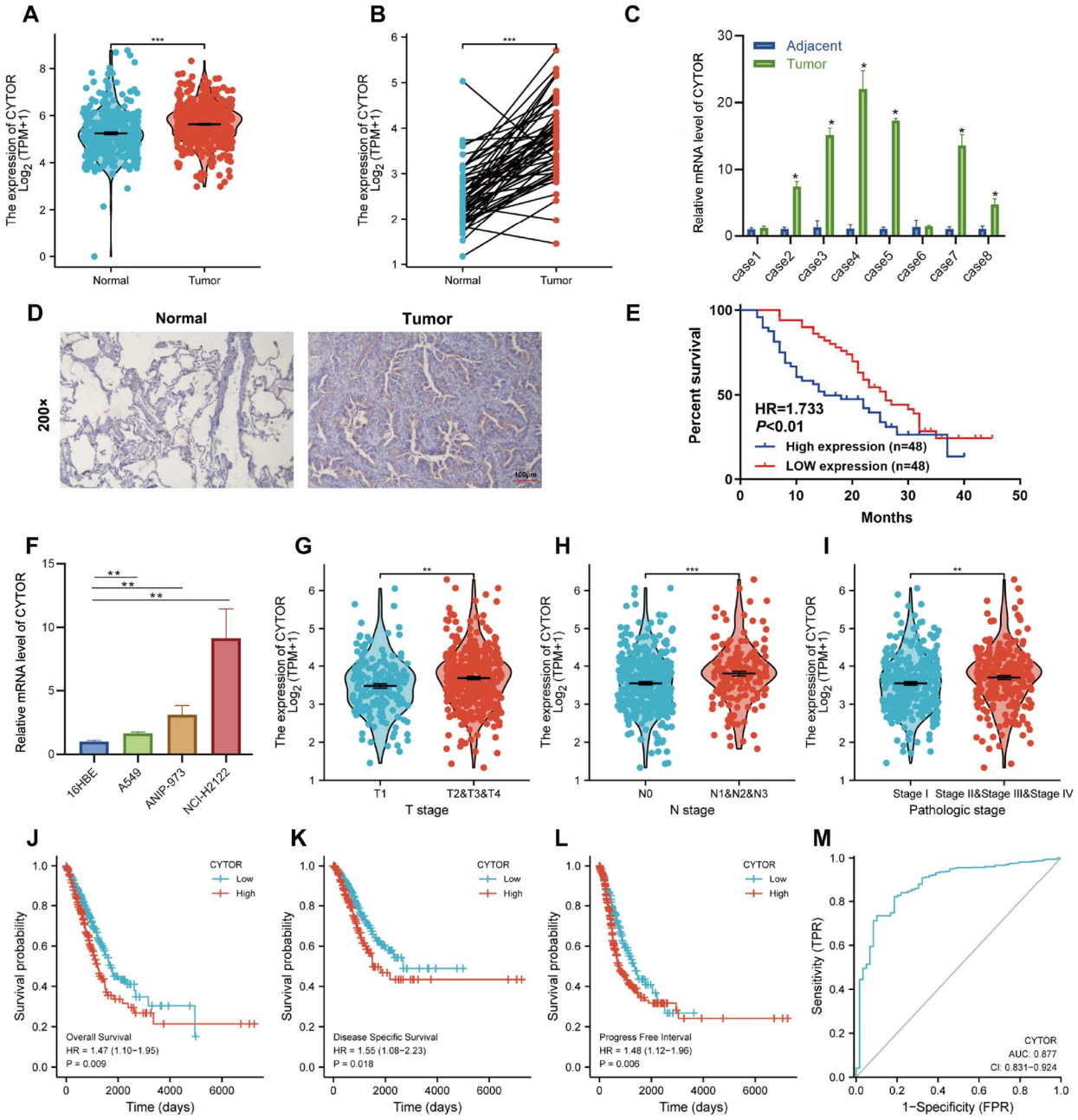

Figure 1. CYTOR is highly expressed and acts as an unfavorable prognostic factor in LUAD (A,B) The expression of CYTOR was summarized in LUAD nonpaired subtypes (A) and paired subtypes (B) from the TCGA database. (C) The expression level of CYTOR in eight paired cancer and adjacent noncancerous tissues was examined by quantitative RT-PCR. (D) CYTOR expression was measured in LUAD and nontumor tissues using *in situ* hybridization technology. (E) Kaplan-Meier survival curves indicate that high expression of CYTOR is associated with poor survival in LUAD patients. (F) CYTOR expression was measured in LUAD cell lines (A549, ANIP-973, and NCI-H2122) and a human bronchial epithelial cell line (16HBE). (G–I) Comparison of CYTOR expression in LUAD patients with different T stages (T2–4 vs T1) (G), N stages (N1–3 vs T0) (H), and pathological stages (stage III & IV vs stage I & II) (I) from the TCGA LUAD subtypes. (J–L) Kaplan-Meier analysis showed that LUAD patients with high CYTOR expression had worse overall survival (J), disease-specific survival (K), and progression-free interval (L). (M) The receiver operating characteristic (ROC) curve of OS-associated CYTOR expression. Data are shown as the mean ± SD, and the experiments were performed three times in triplicate. *$P < 0.05$, **$P < 0.01$, ***$P < 0.001$.

trusted miRNAs were selected. To further reduce the scope of miRNA screening, we used these predicted miRNAs and miRNAs downregulated in LUAD samples (123 miRNAs) to plot the Venn diagram. Then, we obtained five high-confidence miRNAs, including hsa-miR-525-3p, hsa-miR-125b-5p, hsa-miR-125a-5p, hsa-miR-206, and hsa-miR-138-5p (Figure 3A). From the TCGA-LUAD database, we analyzed the correlation of gene expression between CYTOR and these five miRNAs and found that only miR-125a-5p was linearly negatively correlated with CYTOR (Figure 3B). Meanwhile, the expression of miR-125a-5p was significantly lower in TCGA-LUAD tissues than in the paired para-cancerous tissues (Figure 3C). For validation, we conducted quantitative RT-PCR in

Table 1. Clinical characteristics of LUAD patients according to the high and low expression of CYTOR

Characteristics	Number of patients	Expression of CYTOR		*P* value
		Low, *n* (%)	High, *n* (%)	
Age				
≤ 45	35	20 (57.1)	15 (42.9)	0.366
> 45	63	30 (47.6)	33 (52.4)	
Sex				
Male	74	40 (51.4)	34 (45.9)	0.291
Female	24	10 (41.7)	14(58.3)	
T Stage				
T1–T2	47	47 (100)	0 (0)	<0.01
T3–T4	51	3 (5.9)	48 (94.1)	
N Stage				
N0–N1	28	15 (53.6)	13 (46.4)	0.749
N2–N3	70	35 (50)	35 (50)	
TNM Stage				
I–II	14	14 (100)	0 (0)	<0.01
III–IV	84	36 (42.9)	48 (57.1)	
Distant metastasis				
No	77	44 (57.1)	33 (42.9)	0.02
Yes	21	6 (28.6)	15 (71.4)	
Death				
Yes	32	17 (53.1)	15 (469)	0.77
No	66	33 (50)	33 (50)	

LUAD samples and para-cancerous tissues in the eight individual groups and found that miR-125a-5p was significantly downregulated in six of them in lung adenocarcinoma tissues compared with adjacent lung tissues (Figure 3D). The above data demonstrated that miR-125a-5p was downregulated in LUAD. Additionally, we found that miR-125a-5p expression showed a strong correlation with T stage, N stage, and pathological stage, with significantly lower miR-125a-5p level in advanced T stage (Figure 3E), N stage (Figure 3F), and pathological stage (Figure 3G). Survival analysis demonstrated that lower expression of miR-125a-5p was associated with worse overall survival (Figure 3H) and disease-specific survival (Figure 3I). We also found that miR-125a-5p expression decreased in LUAD cell lines (A549 and ANIP-973) compared with that in the bronchial epithelial cell line 16HBE (Figure 3J), indicating that miR-125a-5p may function as a tumor-suppressing miRNA.

Next, to confirm that CYTOR acts as a ceRNA to sponge and downregulate miR-125a-5p, we first evaluated miR-125a-5p expression using quantitative RT-PCR. We found decreased miR-125a-5p expression upon CYTOR overexpression in A549 cells but upregulated miR-125a-5p expression in ANIP-973 cells with *CYTOR* silencing (Figure 3K). Furthermore, we generated dual-luciferase reporters in which CYTOR sequences were predicted to bind with miR-125a-5p (CYTOR WT) and the mutation sequences (CYTOR MUT) were cloned and inserted into pmir-GLO vectors. The results showed that inhibiting miR-125a-5p expression significantly downregulated luciferase activity in the CYTOR WT group, while no change was found in the CYTOR MUT group (Figure 3L). It is known that AGO2 is a vital protein in the RNA-induced silencing complex (RISC), where small RNAs (including miRNAs) load in the RISC and silence target mRNAs. We thus conducted RNA immunoprecipitation using anti-AGO2 antibodies (AGO2-RIP). As shown in Figure 3M, overexpression of miR-125a-5p yielded significant amounts of immunoprecipitated CYTOR RNAs ($P < 0.01$) compared with the negative control group (without miR-125a-5p overexpression). Finally, we transfected biotin-labelled miR-125a-5p into A549 cells and conducted RNA pulldown assays using magnetic streptavidin beads followed by RNA extraction and quantitative RT-PCR analysis. We observed the binding of endogenous CYTOR to this biotin-labelled miR-125a-5p *in vivo* (Figure 3N). Collectively, these data indicated that CYTOR functions via a ceRNA mechanism to sponge miR-125a-5p and inhibits the functions of miR-125a-5p.

ANLN and RRM2 are shared downstream targets of miR-125a-5p

Many studies have proven that miRNAs exert their biological functions by participating in the regulation of their downstream gene translation processes. In mammals, a single mRNA can recognize multiple target mRNAs and bind complementarily to its target, thereby cleaving the mRNAs or preventing the translation of the target genes [25,26]. We then screened the candidate target genes of miR-125a-5p by using PITA (https://genie.weizmann.ac.il/pubs/mir07), RNA22 (https://cm.jefferson.edu/rna22), miRmap (https://mirmap.ezlab.org), and microT (https://www.bio.tools/DIANA-microT#!), miRanda (http://www.microrna.org), PicTar (https://pictar.mdc-berlin.de), and TargetScan (https://www.targetscan.org/vert_72). We found 2739 candidate downstream

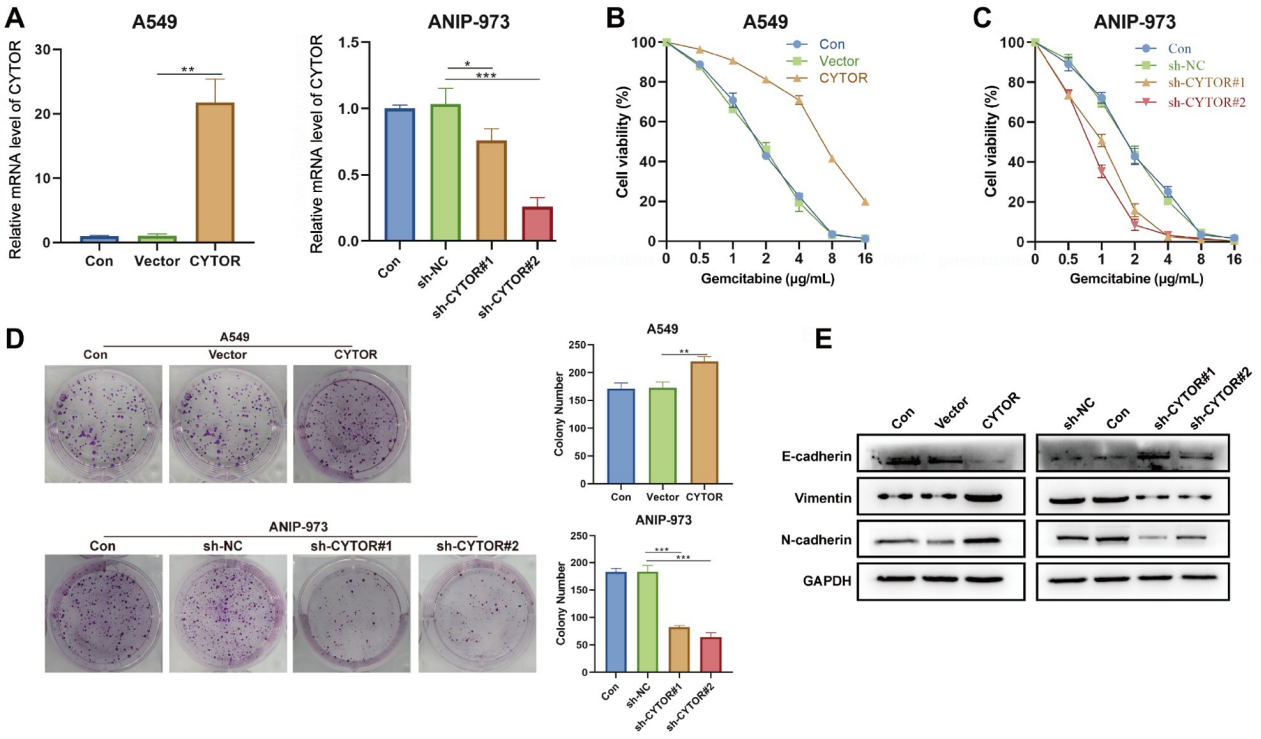

Figure 2. CYTOR contributes to LUAD gemcitabine resistance and endothelial-mesenchymal transition (EMT) *in vitro* (A) CYTOR was overexpressed (CYTOR-overexpressing vectors) in A549 cells (left panel) or silenced (sh-CYTOR#1 and #2) in ANIP-973 cells (right panel). Quantitative RT-PCR was used to confirm the efficiency of knockdown or overexpression. (B,C) A549 (B) and ANIP-973 (C) cells were exposed to culture medium containing different concentrations of gemcitabine (0, 0.5, 1, 2, 4, 8 and 16 μg/mL). Then, cell viability was measured by CCK8 assay. (D) A549 and ANIP-973 cells were exposed to culture medium containing 2 μg/mL gemcitabine. Colony formation experiments were employed to examine the clonal formation ability. (E) Western blot analysis was used to detect the expression levels of vimentin, N-cadherin and E-cadherin in A549 (control or CYTOR-overexpressing) and ANIP-973 (control or sh-CYTOR) cells. Data are shown as the mean ± SD, and the experiments were performed three times in triplicate. $^{*}P < 0.05$, $^{**}P < 0.01$, $^{***}P < 0.001$.

targets of miR-125a-5p. To narrow the range of candidate genes, we took the intersection of these predicted genes with the genes that were upregulated in LUAD tissues from the TCGA dataset and found 122 key target genes (Figure 4A). Among these target genes, *ANLN* and *RRM2* were inversely correlated with miR-125a-5p expression (Figure 4B) and positively associated with CYTOR expression (Figure 4C) according to the TCGA-LUAD dataset, indicating that there may be CYTOR/miR-125a-5p/ANLN and RRM2 regulatory axes in LUAD. To confirm this conjecture, we altered the expression level of miR-125a-5p in A549 and ANIP-973 cells. As shown in Figure 4D, the silencing of miR-125a-5p caused a rapid upregulation of ANLN and RRM2 in A549 cells, while overexpression of miR-125a-5p resulted in the inhibition of ANLN and RRM2 expression in ANLN and RRM2. Furthermore, western blot analysis showed that ANLN and RRM2 were both increased in CYTOR-overexpressing cells but decreased in cells with miR-125a-5p upregulation (Figure 4E). To further elucidate whether ANLN and RRM2 are the target genes of miR-125a-5p, we performed dual-luciferase reporter assay. The binding sites of ANLN and RRM2 were cloned and inserted into the luciferase reporter vector pmirGLO2 (ANLN WT and RRM2 WT). Meanwhile, these binding sequences were mutated (ANLN MUT and RRM2 MUT) to inhibit miR-125a-5p binding. Dual-luciferase assay results showed that overexpression of miR-125a-5p reduced the luciferase activity in the ANLN WT and RRM2 WT groups, while no significant changes were detected in the ANLN MUT and RRM2 MUT groups (Figure 4F–G). Similarly, the AGO2-RIP assay proved that elevated miR-125a-5p expression caused a higher degree of ANLN and RRM2 enrichment in the RISC, illustrating higher levels of miR-125a-5p-mediated ANLN and RRM2 mRNA degradation (Figure 4H). Finally, we confirmed the interaction between miR-125a-5p and ANLN/RRM2 using biotin-labelled miRNA pulldown (Figure 4I). These findings clarified that ANLN and RRM2 are the common downstream genes of miR-125a-5p.

ANLN and RRM2 function as oncogenes in LUAD

Since the above results confirmed that ANLN and RRM2 are involved in the CYTOR/miR-125a-5p regulatory axis, we checked whether ANLN and RRM2 play oncogenic roles in LUAD. We first measured the expression levels of ANLN and RRM2 in LUAD tissues and found that these two genes were both upregulated in LUAD tissues compared with adjacent normal tissues (Figure 5A). As shown in Figure 5B–E, the expressions of ANLN and RRM2 are strongly correlated with the T stage (Figure 5B), N stage (Figure 5C), M stage (Figure 5D), and pathological stage (Figure 5E) in LUAD patients. The above findings indicated that similar to the CYTOR expression pattern, both ANLN and RRM2 were highly expressed in LUAD tissues and indicative of cancer progression. Since miRNA exerts its function through disturbing the translation of target genes, we evaluated the protein expression levels of ANLN and RRM2 using the online tool CPTAC database (https://cptac-data-portal.georgetown.edu/). Compared with those in the normal tissues, both

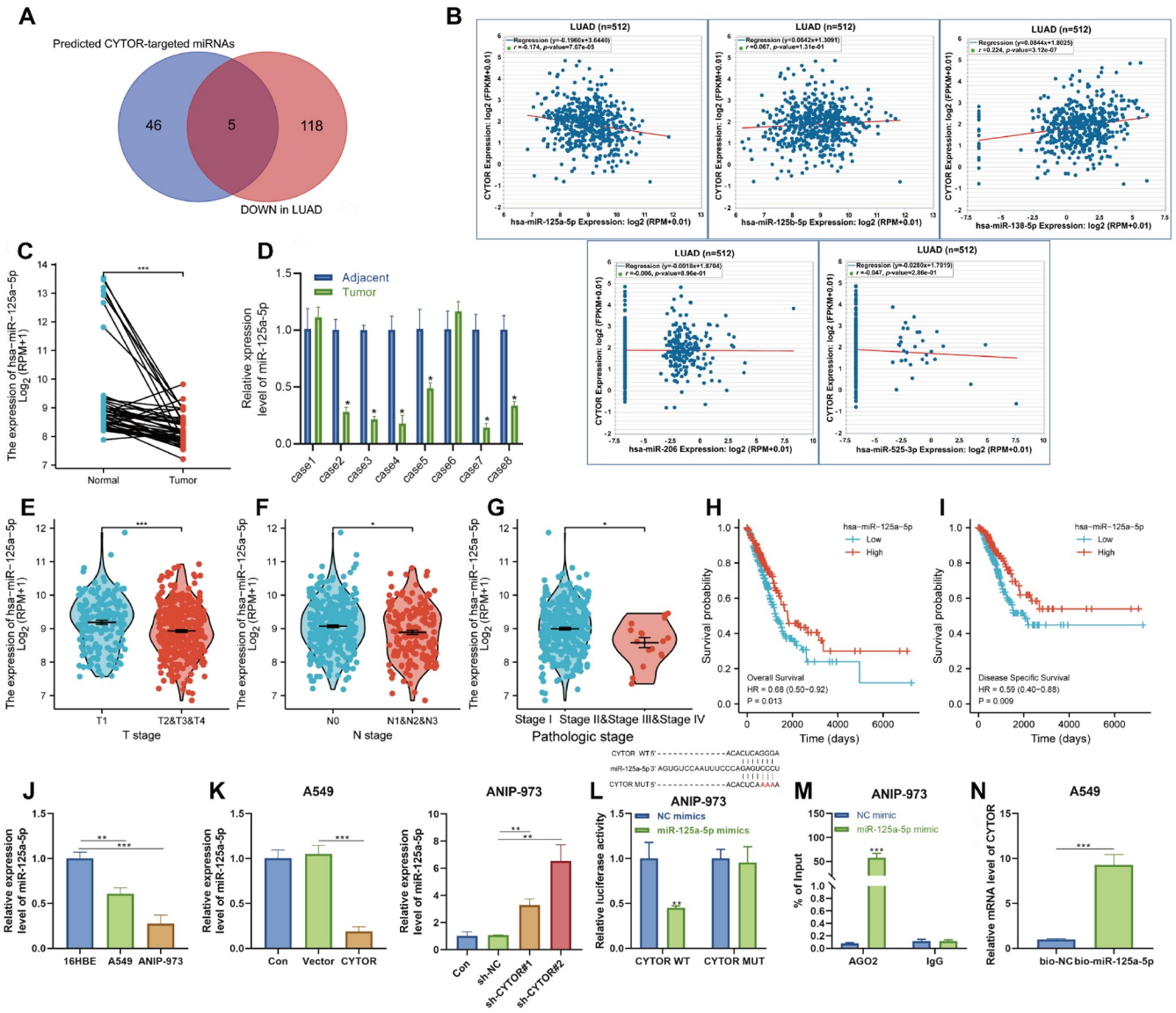

Figure 3. CYTOR acts as a miRNA sponge molecule and absorbs miR-125a-5p (A) Five miRNAs (hsa-miR-525-3p, hsa-miR-125b-5p, hsa-miR-125a-5p, hsa-miR-206, and miR-138-5p) were selected by taking the intersection of the predicted CYTOR-targeting miRNAs and downregulated miRNAs in LUAD samples from TCGA database. (B) Correlation analysis of CYTOR expression with five miRNAs in LUAD samples from the TCGA database. (C) The expression level of miR-125a-5p was evaluated using TCGA paired LUAD samples. (D) Quantitative RT-PCR was used to detect miR-125a-5p expression in eight paired LUAD and adjacent tissues. (E–G) Relationships between miR-125a-5p expression and different T stages (T1 and T2-4) (E) and N stages (N0 and N1-3) (F) were analyzed in TCGA-LUAD samples. (H-I) Overall survival (H) and disease-specific survival (I) curve analysis in TCGA-LUAD patients with low or high miR-125a-5p expression. (J) Differentially expressed miR-125a-5p in LUAD cell lines (A549, ANIP-973, and NCI-H2122) and a human bronchial epithelial cell line (16HBE) is shown. (K) CYTOR was overexpressed in A549 cells or silenced in ANIP-973 cells, and the expression level of miR-125a-5p was measured by quantitative RT-PCR. (L) Dual-luciferase reporter assays were used to detect luciferase activity in ANIP-973 cells overexpressing miR-125a-5p. (M) RNA immunoprecipitation (RIP) of AGO2 followed by quantitative RT-PCR. The amount of miR-125a-5p bound to AGO2 or IgG (control) was measured. (N) RNA pulldown assays using biotin-labelled miR-125a-5p or control probes were performed to determine the enrichment of CYTOR in the lncRNA–miRNA complexes. Data are shown as the mean ± SD, and the experiments were performed three times in triplicate. $*P < 0.05$, $**P < 0.01$, $***P < 0.001$.

ANLN and RRM2 levels were upregulated in the primary tumor (Figure 5F–G, both $P < 0.001$). More importantly, the expressions of ANLN and RRM2 were increased as the tumor grade increased (Figure 5F–G). Subsequently, survival analysis showed that LUAD patients with higher ANLN and RRM2 expressions had shorter overall survival, disease-specific survival, and progression-free survival (Figure 5H–I). We also performed a ROC analysis and calculated the AUC accordingly (Figure 5J). Based on the above results, we conducted *in vitro* functional experiments. Gemcitabine resistance experiments showed that ANLN- and RRM2-overexpressing cells were relatively more resistant to gemcitabine treatment than control cells (Figure 5K). Furthermore, rescue experiments confirmed that ANLN and RRM2 restrained miR-125a-5p-induced gemcitabine sensitivity *in vitro* (Supplementary Figure S1). Collectively, these results illustrated that CYTOR and ANLN/RRM2 have the same phenotypes in LUAD cells.

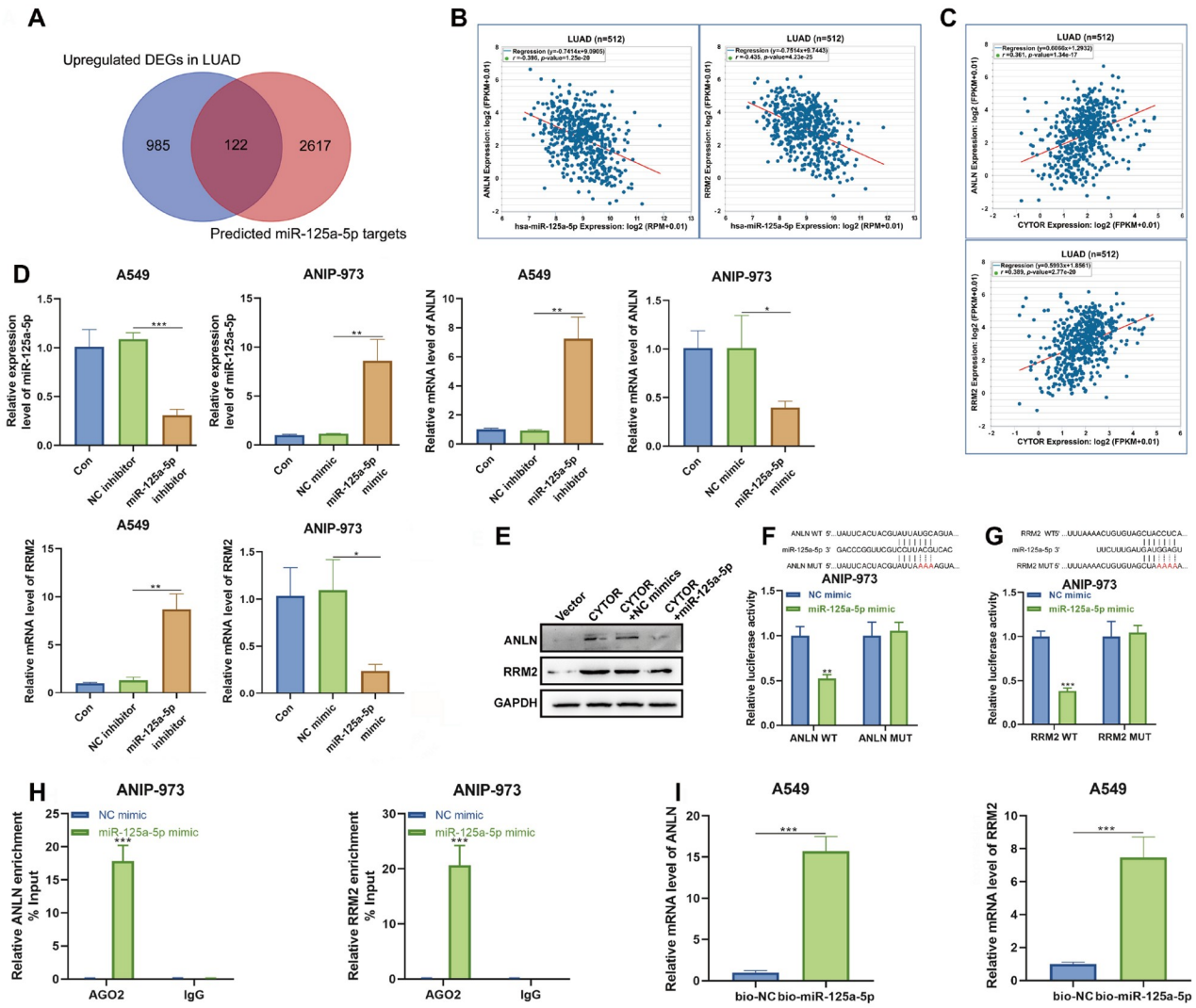

Figure 4. miR-125a-5p binds to ANLN/RRM2 mRNAs and attenuates their expression (A) A total of 122 mRNAs were obtained by taking the intersection of the predicted miR-125a-5p-targeting genes based on online bioinformatics tools (PITA, RNA22, miRmap, microT, miRanda, PicTar, and TargetScan) and genes upregulated in LUAD. (B-C) The associations between ANLN/RRM2 and miR-125a-5p expression (B) and ANLN/RRM2 and CYTOR expression (C) were analyzed using the TCGA-LUAD dataset. (D) Quantitative RT-PCR was performed to measure the expressions of miR-125a-5p, ANLN and RRM2 in A549 cells with miR-125a-5p silencing and in ANIP-973 cells with miR-125a-5p overexpression. (E) Western blot analysis of ANLN and RRM2 expressions in A549 cells transfected with CYTOR- or miR-125a-5p-overexpressing vectors. (F–G) The binding sites and binding mutations of ANLN (ANLN WT and ANLN MUT) (F)/RRM2 (RRM2 WT and RRM2 MUT) (G) with miR-125a-5p were cloned and inserted into the luciferase reporter vector pmirGLO and transfected into ANIP-973 cells. Then, dual-luciferase reporter assays were used to detect luciferase activity in ANIP-973 cells with or without miR-125a-5p overexpression. (H) RIP assays using AGO2 antibodies or normal IgG (negative control) followed by quantitative RT-PCR were performed in ANIP-973 cells with or without miR-125a-5p overexpression. The relative enrichment of ANLN and RRM2 RNAs is shown. (I) Biotin-labelled miRNA pulldowns were conducted to verify the interaction of miR-125a-5p with ANLN and RRM2. Data are shown as the mean ± SD, and the experiments were performed three times in triplicate. $*P<0.05$, $**P<0.01$, $***P<0.001$.

The CYTOR/miR-125a-5p/ANLN and RRM2 axis promotes gemcitabine resistance of LUAD and EMT *in vivo*

To further verify the above *in vitro* findings, we conducted *in vivo* animal experiments. We subcutaneously injected A549 cells with CYTOR-overexpressing or control cells into SPF nude mice (five mice per group) and measured the tumor sizes every week (Figure 6A). We found that A549 cells overexpressing CYTOR grew much faster than the control cells (Figure 6B). Finally, the tumors were measured for size and weight. As shown in Figure 6C, the tumors in the CYTOR-overexpressing group were heavier than those in the control group. To evaluate the influence of CYTOR on gemcitabine resistance *in vivo*, we intraperitoneally administered gemcitabine to nude mice (10 mg/kg) and monitored tumor growth. Consistent with the *in vitro* results, overexpression of CYTOR conferred gemcitabine resistance to A549 cells (Figure 6A–C). Furthermore, we made these tumors into paraffin-embedded sections and performed IHC and TUNEL staining. Immunohistochemistry images showed stronger staining of Ki67, PCNA, ANLN, RRM2 and N-cadherin, but weaker staining of E-cadherin in the CYTOR-overexpressing group than in the control group. These IHC staining indicated stronger proliferation ability and invasive ability in cells overexpressing CYTOR (Figure 6D). Moreover, in the gemcitabine-treated group, fewer TUNEL-positive cells were found in the

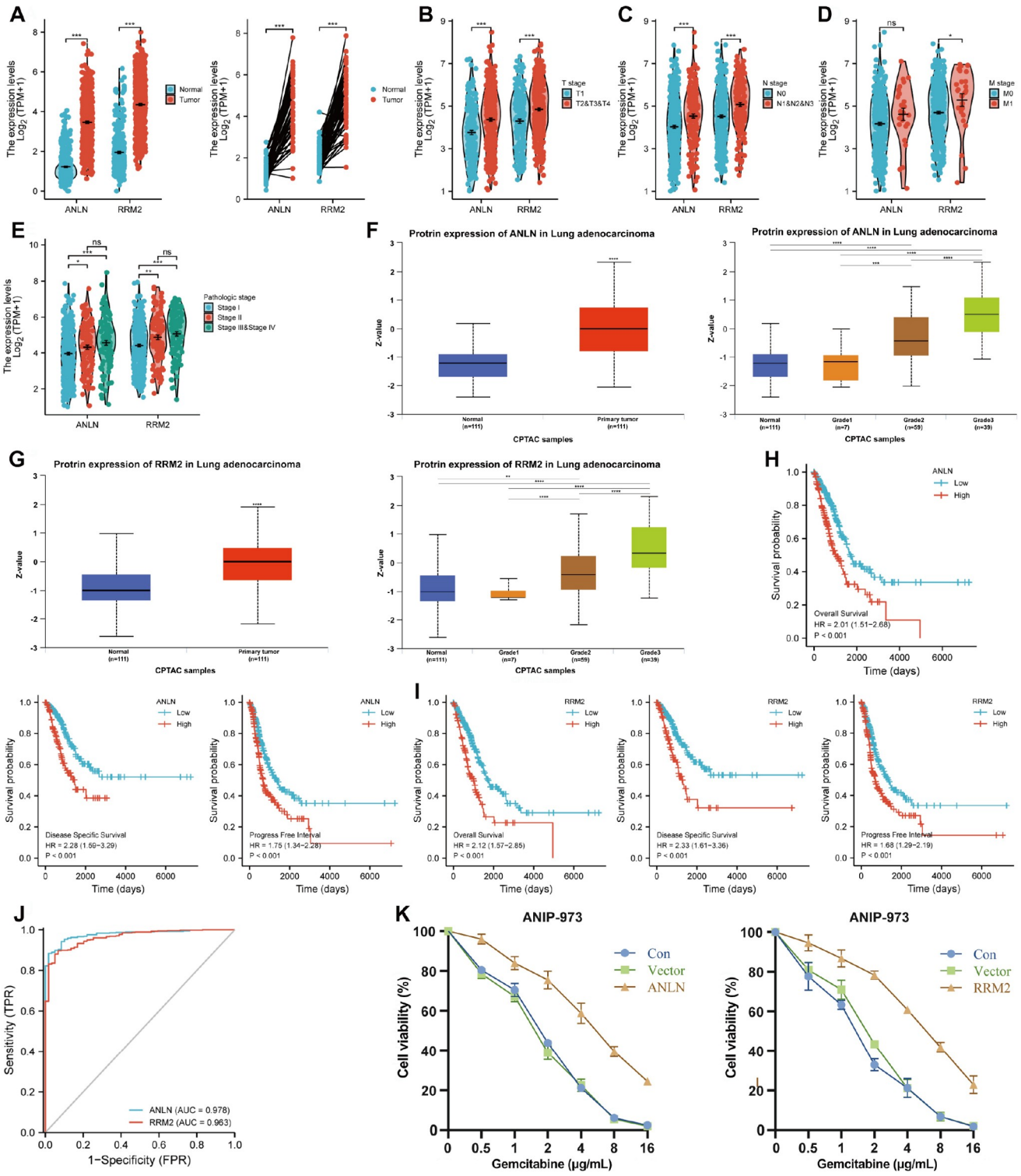

Figure 5. ANLN and RRM2 act as oncogenic genes in LUAD (A) The expression levels of ANLN and RRM2 were analyzed based on LUAD nonpaired (left) and paired (right) subtypes from the TCGA database. (B–E) Comparison of ANLN and RRM2 expression in LUAD patients with different T stages (T1 and T2-4) (B), N stages (N0 and N1-3) (C), M stages (M0 and M1) (D), and pathological stages (I, II and III & IV) (E) from the TCGA LUAD subtypes. (F–G) The protein expression levels of ANLN (F) and RRM2 (G) in LUAD were analyzed according to the CPTAC database. (H–I) Kaplan–Meier survival analysis was employed based on the TCGA database. Overall survival, disease-specific survival, and progression-free survival were analyzed with respect to ANLN (H) and RRM2 (I) expression levels. (J) The receiver operating characteristic (ROC) curve of OS associated with ANLN and RRM2 expression. (K) ANIP-973 cells with ANLN (left) or RRM2 (right) overexpression were exposed to culture medium containing different concentrations of gemcitabine (0, 0.5, 1, 2, 4, 8 and 16 μg/mL). Then, cell viability was measured by CCK8 assay. Data are shown as the mean ± SD, and the experiments were performed three times in triplicate. $*P < 0.05$, $**P < 0.01$, $***P < 0.001$.

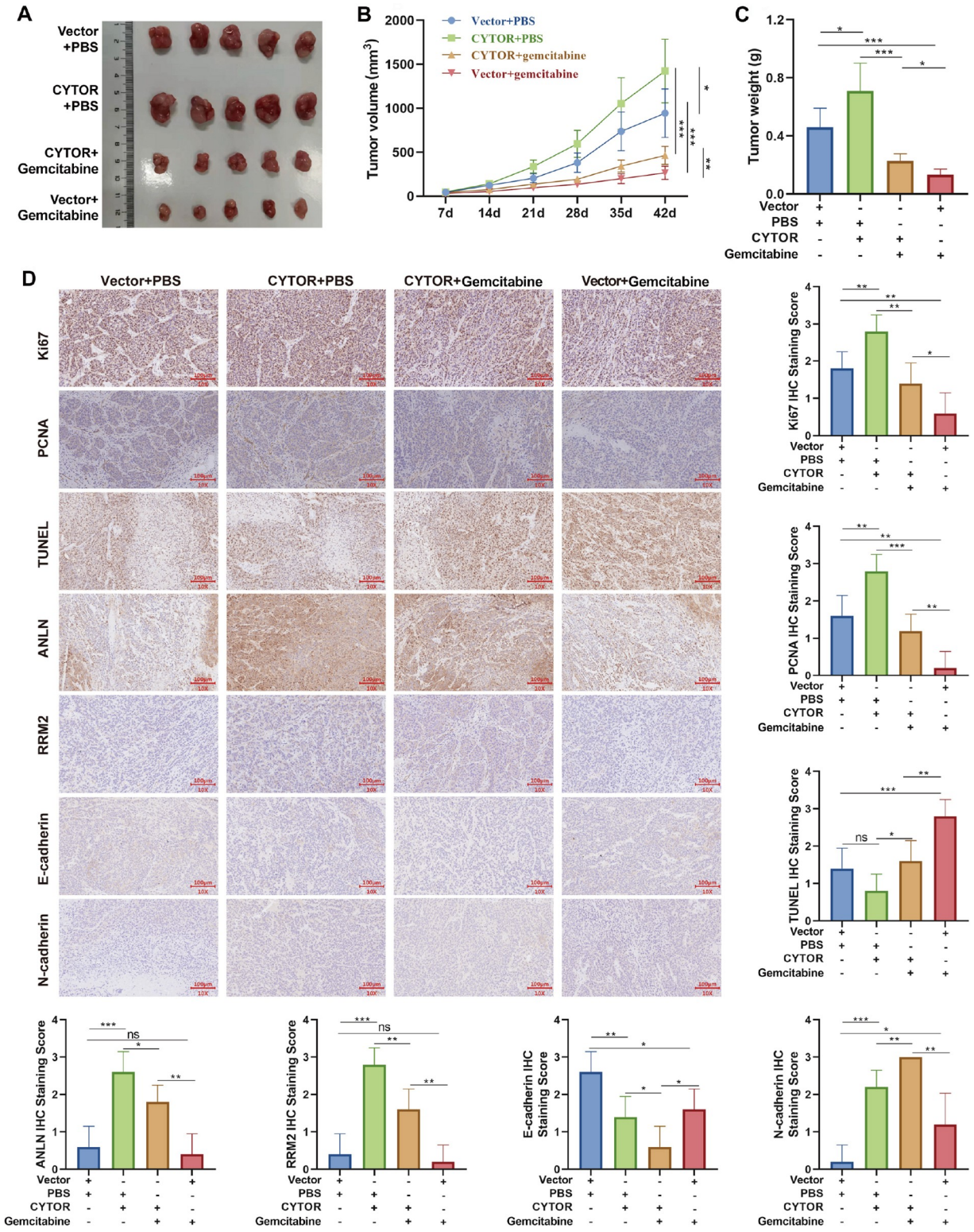

Figure 6. The CYTOR/miR-125a-5p/ANLN and RRM2 axis promotes gemcitabine resistance of LUAD and EMT CYTOR was stably overexpressed in A549 cells. Then, cells with CYTOR overexpression (CYTOR group) or negative control cells (vector group) were subcutaneously implanted into nude mice ($n = 5$ per group). The mice were treated with gemcitabine or PBS (mock treatment) two weeks later (14 d). (A) The volumes of xenograft tumors in nude mice was recorded every week. (B,C) The mice were sacrificed at the sixth week (42 d) and the tumors were isolated. Tumors were imaged (B) and weighed (C). (D) IHC was used to detect Ki67, PCNA, ANLN, RRM2, N-cadherin, E-cadherin and TUNEL expression in paraffin-embedded xenograft tumor sections. (E) Diagram of the molecular mechanism of CYTOR in promoting gemcitabine resistance of LUAD and EMT by sponging miR-125a-5p and upregulating ANLN/RRM2 expression. Data are shown as the mean ± SD, and the experiments were performed three times in triplicate. $^{*}P < 0.05$, $^{**}P < 0.01$, $^{***}P < 0.001$.

CYTOR-overexpressing group than in the control group (Figure 6D), which indicated lower apoptosis level in cells overexpressing CYTOR *in vivo*. In summary, these results confirmed that CYTOR acts as a ceRNA to sponge miR-125a-5p, protects ANLN and RRM2 from miRNA-mediated degradation, and ultimately promotes gemcitabine resistance of LUAD cells and EMT (Figure 6E).

Discussion

Until now, chemoresistance, including gemcitabine resistance, has remained a principal challenge associated with effective treatment for advanced LUAD [27,28]. Although much has been elucidated about the mechanism of chemoresistance in lung cancer, a great deal remains to be evaluated [29]. In addition, developing strategies to resensitize chemoresistant tumors requires a thorough understanding of chemoresistance mechanisms.

Over the past few years, the molecular function of lncRNAs in tumors has attracted increasing attention in the field of noncoding RNAs. Previous studies have shown that lncRNAs are able to bind with DNA, RNA, and protein by its complex secondary structure and complementary pairing with target RNAs (complete or incomplete) and play an essential regulatory role at the epigenetic, transcriptional, and posttranscriptional levels [30–32]. Dysregulation of lncRNAs is ubiquitous in various tumors, and these dysregulated lncRNAs might exert different biological roles, some of which might be tumor suppressors or tumor promoters [33,34]. In this study, we identified an oncogenic lncRNA, CYTOR, which is significantly elevated in LUAD via comprehensive bioinformatics analysis using paired and unpaired TCGA-LUAD datasets. CYTOR is considered to have a tumor-promoting effect in multiple cancers, including breast cancer [35], oral squamous cell carcinoma [36], pancreatic cancer [37], and liver cancer [38]. However, the mechanism of lncRNAs in cancer is complex, and the role of CYTOR in lung cancer has not yet been fully studied. Here, we proved that CYTOR is essential for the gemcitabine resistance and EMT ability of LUAD cells.

In general, the patterns in which lncRNAs exert their functions can be classified into four types, including signal, decoy, guide, and scaffold [18]. Among them, ceRNA, belonging to the decoy mode, has been widely demonstrated in multiple tumor types [39,40]. As is known to us, miRNAs are able to bind to their target mRNAs, inhibiting their translation or causing mRNA degradation, thus realizing the function of posttranscriptional regulation of gene expression. The same miRNA can bind to multiple RNAs, and a competitive relationship is formed between these RNA molecules that bind to the same miRNA. Therefore, lncRNAs can inhibit the effect of miRNAs by binding to miRNAs and competing with their target mRNAs [41–43]. In gastric cancer (GC), LINC01133 is downregulated and acts as a key tumor suppressor to inhibit GC progression and metastasis. As a ceRNA, LINC01133 plays a role by absorbing miR-106a-3p, upregulating APC expression, and finally activating the Wnt/β-catenin pathway [44]. PCAT6 is a novel lncRNA induced by M2 macrophages from the tumor microenvironment. PCAT6 boosts breast cancer growth and microangiogenesis by interacting with miR-4723-5p and upregulating VEGFR2 [45]. Similarly, the lncRNA–miRNA-mRNA interaction network is also involved in the tumorigenesis and progression of lung cancer. For example, LINC00336 serves as a ceRNA to bind with miR-6852 and upregulate CBS, a surrogate marker of ferroptosis, and promotes tumor cell proliferation by inhibiting ferroptosis [46]. In the present study, by integrating multiple external databases and bioinformatics analysis tools (such as PITA, RNA22, miRmap, microT, miRanda, PicTar, and TargetScan), we identified miR-125a-5p as one of the high confidence lists of candidate miRNAs. Subsequently, the direct interaction between miR-125a-5p and CYTOR was experimentally determined by dual-luciferase reporter assay, RNA immunoprecipitation, and biotin-labelled RNA pulldown assay. We finally confirmed that CYTOR acts as a ceRNA to absorb miR-125a-5p, inhibits ANLN and RRM2 mRNA degradation, and ultimately confers LUAD cell stronger gemcitabine resistance and EMT ability.

Supplementary Data

Supplementary Data is available at Acta Biochimica et Biophysica Sinica online.

Funding

This work was supported by the grants from the National Natural Science Foundation of China (Nos. 82072725 and 81872042 to X. C.),

Conflict of Interest

The authors declare that they have no conflict of interest.

References

1. Lambe G, Durand M, Buckley A, Nicholson S, McDermott R. Adenocarcinoma of the lung: from BAC to the future. *Insights Imag* 2020, 11: 69
2. Succony L, Rassl DM, Barker AP, McCaughan FM, Rintoul RC. Adenocarcinoma spectrum lesions of the lung: detection, pathology and treatment strategies. *Cancer Treatment Rev* 2021, 99: 102237
3. Kuhn E, Morbini P, Cancellieri A, Damiani S, Cavazza A, Comin CE: Adenocarcinoma classification: patterns and prognosis. *Pathologica* 2018, 110: 5–11
4. Denisenko TV, Budkevich IN, Zhivotovsky B. Cell death-based treatment of lung adenocarcinoma. *Cell Death Dis* 2018, 9: 117
5. Liu Y, Li Y, Wang X, Liu F, Gao P, Quinn MM, Li F, *et al.* Gemcitabine and Chk1 inhibitor AZD7762 synergistically suppress the growth of Lkb1-deficient lung adenocarcinoma. *Cancer Res* 2017, 77: 5068–5076
6. Han JY, Park K, Kim SW, Lee DH, Kim HY, Kim HT, Ahn MJ, *et al.* First-SIGNAL: first-line single-agent iressa versus gemcitabine and cisplatin trial in never-smokers with adenocarcinoma of the lung. *J Clin Oncol* 2012, 30: 1122–1128
7. Mini E, Nobili S, Caciagli B, Landini I, Mazzei T. Cellular pharmacology of gemcitabine. *Ann Oncol* 2006, 17: v7–v12
8. Gesto DS, Cerqueira NM, Fernandes PA, Ramos MJ. Gemcitabine: a critical nucleoside for cancer therapy. *Curr Med Chem* 2012, 19: 1076–1087
9. Bergman AM, Pinedo HM, Peters GJ. Determinants of resistance to 2′,2′-difluorodeoxycytidine (gemcitabine). *Drug Resist Updat* 2002, 5: 19–33
10. St. Laurent G, Wahlestedt C, Kapranov P. The Landscape of long noncoding RNA classification. *Trends Genet* 2015, 31: 239–251
11. Kopp F, Mendell JT. Functional classification and experimental dissection of long noncoding RNAs. *Cell* 2018, 172: 393–407
12. Schmitz SU, Grote P, Herrmann BG. Mechanisms of long noncoding RNA function in development and disease. *Cell Mol Life Sci* 2016, 73: 2491–2509
13. Bhan A, Soleimani M, Mandal SS. Long noncoding RNA and cancer: a new paradigm. *Cancer Res* 2017, 77: 3965–3981
14. Huang Z, Zhou JK, Peng Y, He W, Huang C. The role of long noncoding RNAs in hepatocellular carcinoma. *Mol Cancer* 2020, 19: 77

15. Amelio I, Bernassola F, Candi E. Emerging roles of long non-coding RNAs in breast cancer biology and management. *Semin Cancer Biol* 2021, 72: 36–45
16. Luo X, Qiu Y, Jiang Y, Chen F, Jiang L, Zhou Y, Dan H, *et al.* Long non-coding RNA implicated in the invasion and metastasis of head and neck cancer: possible function and mechanisms. *Mol Cancer* 2018, 17: 14
17. Wei L, Sun J, Zhang N, Zheng Y, Wang X, Lv L, Liu J, *et al.* Noncoding RNAs in gastric cancer: implications for drug resistance. *Mol Cancer* 2020, 19: 62
18. Hosseini ES, Meryet-Figuiere M, Sabzalipoor H, Kashani HH, Nikzad H, Asemi Z. Dysregulated expression of long noncoding RNAs in gynecologic cancers. *Mol Cancer* 2017, 16: 107
19. Lu L, Liu LP, Zhao QQ, Gui R, Zhao QY. Identification of a ferroptosis-related lncRNA signature as a novel prognosis model for lung adenocarcinoma. *Front Oncol* 2021, 11: 675545
20. Qian X, Yang J, Qiu Q, Li X, Jiang C, Li J, Dong L, *et al.* LCAT3, a novel m6A-regulated long non-coding RNA, plays an oncogenic role in lung cancer via binding with FUBP1 to activate c-MYC. *J Hematol Oncol* 2021, 14: 112
21. Zou SF, Yang XY, Li JB, Ding H, Bao YY, Xu J. UPF1 alleviates the progression of glioma via targeting lncRNA CYTOR. *Eur Rev Med Pharmacol Sci* 2019, 23: 10005–10012
22. Li M, Wang Q, Xue F, Wu Y. lncRNA-CYTOR works as an oncogene through the CYTOR /miR-3679-5p/ MACC1 axis in colorectal cancer. *DNA Cell Biol* 2019, 38: 572–582
23. Silahtaroglu AN, Nolting D, Dyrskjøt L, Berezikov E, Møller M, Tommerup N, Kauppinen S. Detection of microRNAs in frozen tissue sections by fluorescence in situ hybridization using locked nucleic acid probes and tyramide signal amplification. *Nat Protoc* 2007, 2: 2520–2528
24. Tay Y, Rinn J, Pandolfi PP. The multilayered complexity of ceRNA crosstalk and competition. *Nature* 2014, 505: 344–352
25. Hammond SM. An overview of microRNAs. *Adv Drug Deliver Rev* 2015, 87: 3–14
26. Di Leva G, Garofalo M, Croce CM. MicroRNAs in cancer. *Annu Rev Pathol Mech Dis* 2014, 9: 287–314
27. Lim ZF, Ma PC. Emerging insights of tumor heterogeneity and drug resistance mechanisms in lung cancer targeted therapy. *J Hematol Oncol* 2019, 12: 134
28. Wang M, Herbst RS, Boshoff C. Toward personalized treatment approaches for non-small-cell lung cancer. *Nat Med* 2021, 27: 1345–1356
29. Rotow J, Bivona TG. Understanding and targeting resistance mechanisms in NSCLC. *Nat Rev Cancer* 2017, 17: 637–658
30. Peng WX, Koirala P, Mo YY. LncRNA-mediated regulation of cell signaling in cancer. *Oncogene* 2017, 36: 5661–5667
31. Ferrè F, Colantoni A, Helmer-Citterich M. Revealing protein–lncRNA interaction. *Brief Bioinform* 2016, 17: 106–116
32. Statello L, Guo CJ, Chen LL, Huarte M. Gene regulation by long non-coding RNAs and its biological functions. *Nat Rev Mol Cell Biol* 2021, 22: 96–118
33. Tan YT, Lin JF, Li T, Li JJ, Xu RH, Ju HQ. LncRNA-mediated posttranslational modifications and reprogramming of energy metabolism in cancer. *Cancer Commun* 2021, 41: 109–120
34. Schmitt AM, Chang HY. Long noncoding RNAs in cancer pathways. *Cancer Cell* 2016, 29: 452–463
35. Liu Y, Li M, Yu H, Piao H. lncRNA CYTOR promotes tamoxifen resistance in breast cancer cells via sponging miR-125a-5p. *Int J Mol Med* 2020, 45: 497–509
36. Zhu W, Wang J, Liu X, Xu Y, Zhai R, Zhang J, Wang M, *et al.* lncRNA CYTOR promotes aberrant glycolysis and mitochondrial respiration via HNRNPC-mediated ZEB1 stabilization in oral squamous cell carcinoma. *Cell Death Dis* 2022, 13: 703
37. Zhu H, Shan Y, Ge K, Lu J, Kong W, Jia C. LncRNA CYTOR promotes pancreatic cancer cell proliferation and migration by sponging miR-205-5p. *Pancreatology* 2020, 20: 1139–1148
38. Tian Q, Yan X, Yang L, Liu Z, Yuan Z, Zhang Y. lncRNA CYTOR promotes cell proliferation and tumor growth via miR-125b/SEMA4C axis in hepatocellular carcinoma. *Oncol Lett* 2021, 22: 796
39. Qi X, Zhang DH, Wu N, Xiao JH, Wang X, Ma W. ceRNA in cancer: possible functions and clinical implications. *J Med Genet* 2015, 52: 710–718
40. Karreth FA, Pandolfi PP. ceRNA cross-talk in cancer: when ce-bling rivalries go awry. *Cancer Discov* 2013, 3: 1113–1121
41. Thomson DW, Dinger ME. Endogenous microRNA sponges: evidence and controversy. *Nat Rev Genet* 2016, 17: 272–283
42. Zhang Y, Song D, Peng Z, Wang R, Li K, Ren H, Sun X, *et al.* LINC00891 regulated by miR-128-3p/GATA2 axis impedes lung cancer cell proliferation, invasion and EMT by inhibiting RhoA pathway. *Acta Biochim Biophys Sin* 2022, 54: 378–387
43. Wei F, Wang Y, Zhou Y, Li Y. Long noncoding RNA CYTOR triggers gastric cancer progression by targeting miR-103/RAB10. *Acta Biochim Biophys Sin* 2021, 53: 1044–1054
44. Yang XZ, Cheng TT, He QJ, Lei ZY, Chi J, Tang Z, Liao QX, *et al.* LINC01133 as ceRNA inhibits gastric cancer progression by sponging miR-106a-3p to regulate APC expression and the Wnt/β-catenin pathway. *Mol Cancer* 2018, 17: 126
45. Dong F, Ruan S, Wang J, Xia Y, Le K, Xiao X, Hu T, *et al.* M2 macrophage-induced lncRNA PCAT6 facilitates tumorigenesis and angiogenesis of triple-negative breast cancer through modulation of VEGFR2. *Cell Death Dis* 2020, 11: 728
46. Wang M, Mao C, Ouyang L, Liu Y, Lai W, Liu N, Shi Y, *et al.* Correction to: Long noncoding RNA LINC00336 inhibits ferroptosis in lung cancer by functioning as a competing endogenous RNA. *Cell Death Differ* 2020, 27: 1447